Research on the Construction Mechanics and Stability Control Technology of Expressway Tunnel Based on Numerical Analysis

Wei Li and Hongping Wen*

College of Engineering Management, Shanxi Vocational University of Engineering Science and Technology, Jinzhong 030600, China
E-mail: 5770722@qq.com
**Corresponding Author*

Received 26 June 2024; Accepted 09 August 2024

Abstract

As an effective structural form, connecting arch tunnel has been widely used in practical engineering because of its smooth linear shape, small footprint and good bridge and tunnel connection. With the increase of domestic traffic volume year by year, the width of the even arch tunnel is gradually changed from two-way four lanes to two-way six lanes. I20 I-steel, spacing 0.75∼1 m, anchor length 3∼4 m, ring spacing 0.5∼1 m, the side ring spacing of the middle wall is 0.75 m, the side ring spacing of the side wall is 1 m, and the shotcrete thickness is 0.25∼0.3 m. The excavation span of a two-way six-lane continuous-arch tunnel is considerable, leading to complex stress characteristics, thereby posing risks to construction safety and structural stability. Following the construction of the initial tunnel, disturbance to the surrounding rock occurs, affecting subsequent excavation phases. The initial support requirements for subsequent excavations are more intricate, with increased internal forces compared to the initial tunnel segment. As the rear tunnel progresses, the surrounding rock near the middle wall shifts

European Journal of Computational Mechanics, Vol. 33_5, 461–482.
doi: 10.13052/ejcm2642-2085.3352

towards the rear tunnel, reducing internal forces in the concrete and steel arch frame. However, as the rear tunnel distance increases, concrete stress and axial forces on the middle wall side of the initial tunnel begin to rise. Throughout the construction, the steel arch frame's internal forces and spray concrete stress on the middle wall side's arch waist and foot are the highest, making them susceptible to disruption from construction on the opposite side, thus constituting critical tunnel components. Numerical simulations effectively capture surrounding rock and structural stress dynamics during large-span arch tunnel construction. Simulation outcomes align closely with field measurements, particularly in three-dimensional simulations, enhancing construction understanding and management.

Keywords: Large span, connecting arch tunnel, 3D simulation, numerical analysis, middle wall.

1 Introduction

Currently, China's high-grade highway construction is experiencing rapid growth, necessitating numerous tunnel projects. Traditionally, tunnel design adopts a double-hole separation approach [1]. However, in regions with unique geological and topographic constraints, continuous arch tunnel schemes have emerged as the preferred choice for tunnel design and construction. This trend is evident in numerous highway projects across the country, including those under construction and proposed. Moreover, with the burgeoning development of municipal infrastructure, significant underground traffic and municipal engineering projects are underway in large and medium-sized cities, particularly in crucial transportation hubs and busy areas [2, 3]. These projects frequently feature arch and arch structures, reflecting a substantial portion of the engineering endeavors in these urban landscapes. For example, Beijing Second Ring Road Tunnel of Urban Railway; Liuzhou Tongyou Mountain Tunnel; Nanjing Gulou Tunnel; Guangzhou Baiyun Mountain Tunnel; Beijing Gaobeidian three arch drainage tunnel, etc. Underground railway has gradually become an important part of the large and medium-sized urban rail transit system. In the large transfer station, station of the underground railway, the tunnel crossing section and part of the tunnel. Such as Beijing subway in Xidan subway station [4, 5].

The number of connecting arches and connecting arch structures under construction or planned in China ranks first in the world, and there are many connecting arch tunnels built before in the form of two-way four lanes. With

the arrival of a new round of infrastructure construction, especially the climax of western development, the design of two-way four-lane expressway gradually cannot meet the requirements of economic development [6, 7]. In recent years, more and more two-way six-lane expressway in China, and the construction of two-way six-lane highway tunnel is also increasing. At present, Chongqing, Beijing, Guangdong, Jiangsu, Yunnan and other provinces and cities have built zhenwu Mountain tunnel, Buddha Temple tunnel, Yangzong tunnel, Beijing-Zhuhai Expressway South section of longling tunnel, Yunnan Kunming-Shi Expressway No.1 tunnel, Ning-Hangzhou expressway six-lane highway tunnel [8, 9]. The construction of domestic two-way six-lane continuous arch highway tunnel is still in its initial stage, and there are few design and construction experience for reference. Different from the four-lane connected-arch tunnel, the common excavation span of the six-lane connected-arch highway tunnel is about 32 m, its maximum height is about 12 m, and the minimum single-arch vector span ratio is 0.45. The tunnel section and span are relatively large, and the section is flat, which has adverse effects on the safety and structural stability of the tunnel construction [10, 11]. Currently for large span arch tunnel design parameters of supporting structure is conservative, but due to the large across the arch tunnel construction method is complex, the construction process is more, due to the need to set up temporary support and make the construction appear repeatedly, this not only seriously affect the tunnel construction progress, and supporting structure is prone to relatively weak parts [12, 13].

2 Tunnel Surrounding Rock and Structure On-site

2.1 Tunnel Geological Conditions

Directly exposed. As shown in formula (1), the hillside slope is 20–30, and the ridge direction is basically perpendicular to the tunnel axis.

$$F_n(t) = e^{-\lambda t}, (n = 1, 2, \ldots, N + X) \tag{1}$$

The upper part of the ridge is steep and the lower part is slow; the inlet is slow and the outlet is steep, and the tunnel site area is mainly Cretaceous fine sandstone with thin mudstone. As shown in formula (2), the whole-strongly weathered rock mass is micro-fragmented, and fragmented.

$$F_{N/(N+X)}(t) = \sum_{n=N}^{N+X} C_{N+X}^{N} e^{-n\lambda t} (1 - e^{-\lambda t})^{N+X-n} \tag{2}$$

The tunnel site belongs to the eastern section of the Qinling structural belt, and the fault structure is relatively developed. Wujiazhuang tunnel is 340 m long, with a span of 32.61 m, high 11.28 m and a maximum buried depth of 75 m. Import pile number is K41 + 640, exit pile number is K41 + 980, K41 + 640∼655 and K41 + 960∼980 section is open hole, as shown in formula (3), the design of composite lining, initial support by system bolt, single layer steel mesh, shotcrete, I-word steel arch, combined with advance small pipe, mold C25 reinforced concrete as secondary lining, middle wall using three layers straight middle wall, wall height of 7.56m, total thickness of 2.4 m, two outer layers for secondary lining.

$$u_{ok} = u_{ik} - L_f \frac{di_{Lk}}{dt} - R_L i_{Lk} \tag{3}$$

The supporting parameters of grade V surrounding rock are as follows: 30 cm thick C25 shotcrete for the initial lining, I25a steel arch spacing is 75 cm, the secondary lining thickness is 50 cm. As shown in formula (4), the surrounding rock surrounding convergence measurement:

$$i_{Lk} = i_{ok} + C_f \frac{du_{ok}}{dt} \tag{4}$$

Internal force of the middle use steel wire concrete strain measurement to measure the vertical stress in the upper. As shown in formula (5), measure the internal force of the full section steel arch. Radial force measurement of shotcrete: use steel wire concrete strain measurement to measure the radial stress.

$$G_{LC}(s) = \frac{\omega_n^2}{s^2 + 2\zeta\omega_n s + \omega_n^2} \tag{5}$$

Tangential stress measurement of shotcrete: using steel wire concrete strain measurement. As shown in formula (6).

$$10 f_0 < \frac{1}{2\pi\sqrt{L_f C_f}} < \frac{1}{10} f_s \tag{6}$$

2.2 Steel Supports Internal Forces

Due to various foreseeable or unforeseeable reasons, the data measured by the field measurement has certain dispersion, so the error analysis, regression analysis and induction, as shown in Equation (7), can well explain the

meaning of the measurement results and make full use of the results of the measurement analysis.

$$i_{on} = I_n \angle \phi_n = \frac{U_n \angle \varphi_n - U_{\text{load}} \angle 0^\circ}{Z_{on}} \tag{7}$$

For example, to understand the change rate of displacement at a certain point at a certain time, it is not accurate to simply subtract the data measured at a neighboring time by the time interval as the change rate, as shown in Equation (8), the correct method is to measure the displacement array to the time-displacement curve.

$$P_n = \frac{1}{X_{on}}(U_{load} U_n sin\varphi_n) \tag{8}$$

In short, the purpose of the mathematical processing of measurement data is verification, feedback and prediction. In the process of measuring the data, we should pay attention to complete the following contents at any time: to confirm the measurement data with each other to confirm the reliability of the measurement results as shown in Equation (9).

$$\begin{cases} f_1 = f_{01} - k_{P1} P_1 \\ f_2 = f_{02} - k_{P2} P_2 \end{cases} \tag{9}$$

Theoretically speaking, a reasonable and reliable support system should be that all the physical quantities representing the rock. As shown in Equation (10), on the contrary, if some or some physical quantities, and the design parameters must be strengthened or modified to achieve the purpose of information design.

$$\begin{cases} U_1 = U_{01} - k_{Q1} Q_1 \\ U_2 = U_{02} - k_{Q2} Q_2 \end{cases} \tag{10}$$

In the primary lining concrete of the test section K41 + 894,12 concrete strain meters are buried. The buried instruments are expressed by C9∼C20. As shown in Equation (11), the concrete strain gauge is directly tied to the primary lining along the tunnel tangential direction before the shotcrete.

$$\Delta P = \frac{|f_1 - f_2|}{k_P} \tag{11}$$

Within a few days after the embedding of the instrument, due to the concrete solidification process resulting in the heat of hydration, the internal temperature is relatively high, and at this time the concrete strength and elastic modulus are relatively low, as shown in formula (12), the strain generated by the concrete strain gauge in this stage is not mainly caused by the concrete force,

$$f = f_0 - k_P P - k_{Pd}\frac{dP}{dt} \tag{12}$$

3 Numerical Simulation of a Large-span Continuous-arch Tunnel

3.1 Flac Fundamental

Following the excavation of steps in the left and right holes, there is a 55 m increase in concrete stress, stabilizing thereafter. Upon cutting off the steel arch frame of the middle guide tunnel, the concrete stress decreases in the left hole, with slight reductions observed in the arch roof and arch waist of the right hole, while other areas remain unchanged [14]. Lowering the steps in the left hole leads to a roughly 10% increase in concrete stress for both holes. Subsequent excavation of the right hole results in a 3% decrease in concrete stress for the left hole and a further increase ranging between 9% and 14% for the right hole. As the second lining approaches in the left hole, primary lining concrete stress begins to decline. Following the second lining, there is a 3% to 12% increase in stress and maximum stress levels [15, 16]. When applied as the second lining of the right hole, The initial lining concrete stress of the left hole has small fluctuations, The concrete stress in the right hole has changed, And reach the maximum stress value two days after pouring the second lining of the section, Figure 1 shows the concrete stress assessment drawing of the two-hole arch, Different ratio of the increase to the maximum stress, The maximum amount of change is the vault, Up to 5.3 MPa, And the maximum stress ratio of 49%, The minimum arch foot part on both sides, At about 10%, The stress slowly recovered after ten days [17, 18], The stress of the bilateral arch feet returns to the original stress value. In the following year, In the first half of the year, the stress of the two holes increases and reaches the maximum value [19, 20].

The concrete elastic mold is gradually increasing. When the main holes of the upper steps on both sides are excavated, the concrete stress increases at another speed, and the increase speed slows down. Figure 2 shows the FLAC

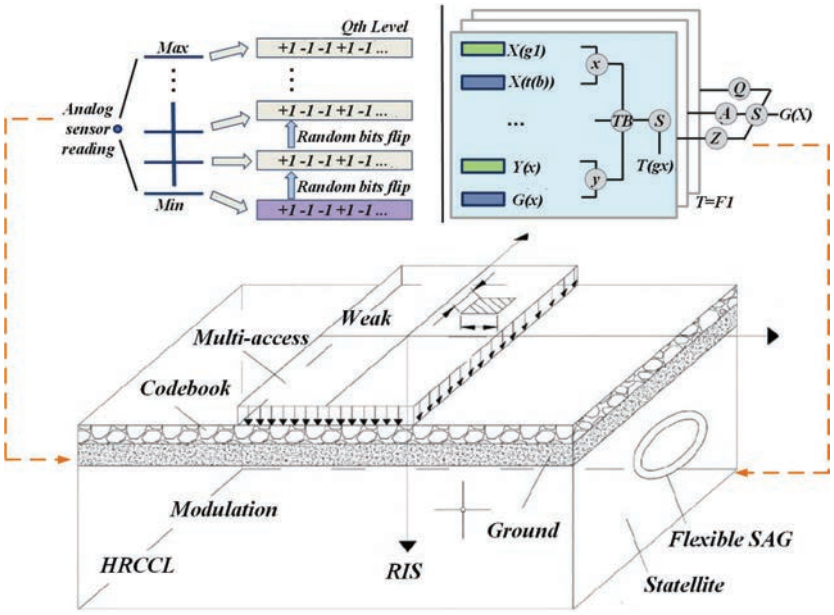

Figure 1 Concrete stress assessment drawing of the arch of the two holes.

principle of the primary lining concrete. When the second lining of the left hole is poured, the radial stress of the concrete suddenly decreases, and the reduction is large, and the maximum stress proportion is 61%. After over ten days, it gradually returned to the original stress value of [21, 22]. In a year after the second lining measurement can see, in the first half, may be because the first lining and the second lining between waterproof board, the first lining and two lining without dense contact, the first lining will gradually deformation, internal stress gradually adjust, so in the first half of the stress will gradually smaller, to the second half of the first lining and two lining contact completely, the first lining stress with the increase of surrounding rock stress and gradually increase [23].

Throughout the construction process, the primary lining concrete consistently experiences tensile stress, with a maximum of 2.24 MPa. Radial stress in the primary lining concrete rises only during side guide tunnel excavation and upper step construction. There's a slight reduction during lower step excavation, reaching its peak just before lower step excavation begins. It can also be seen that the construction on the other side does not significantly affect the concrete radial stress of the side wall [24, 25]. When the steps on the

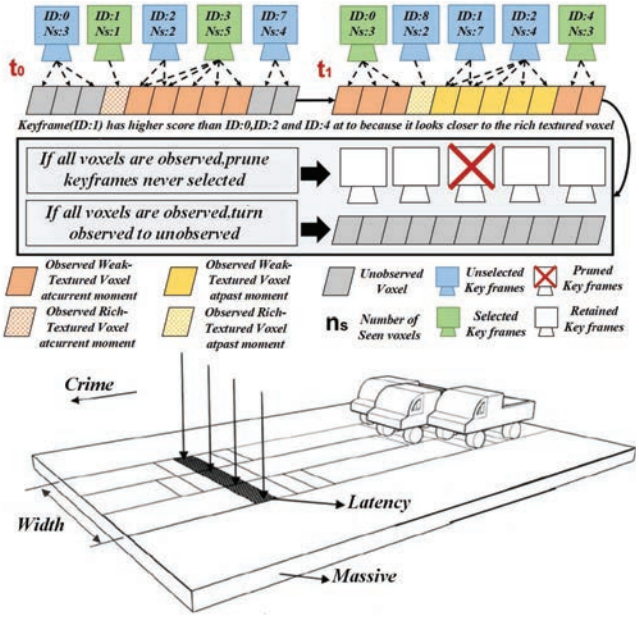

Figure 2 Flac principle of primary lining concrete.

right hole are excavated to 5 m away from the test section, the stress on both sides of the middle wall increases at a fast rate of [26, 27]. The stress on both sides of the middle wall is reduced. Final right hole two lining pouring, the wall on the right, middle and lower stress is 3.04 MPa, 3.15 MPa, 4.49 MPa respectively, and the left part of the stress is 13.64 MPa, 6.25MPa, 5.62 MPa, visible in the wall left the lower stress is the lowest [28], the middle second, the largest, and the wall right lower stress, the middle second, the smallest, even arch tunnel construction, the wall and the lower ends are end effect.

3.2 Three-Dimensional Simulation

Following the excavation of the lower steps in the left hole, the axial force pulling on the arch section of both holes diminishes, while the axial force pressing on other sections increases. Notably, the axial force on the steel arch's foot in the left hole undergoes the most significant change. Subsequently, as the right hole undergoes lower step excavation, the axial force in the left hole continues to rise, with minimal change observed in the axial force of the vault and sidewall of the right hole. Meanwhile, the axial force on other sections increases. Throughout the lower step excavation process on

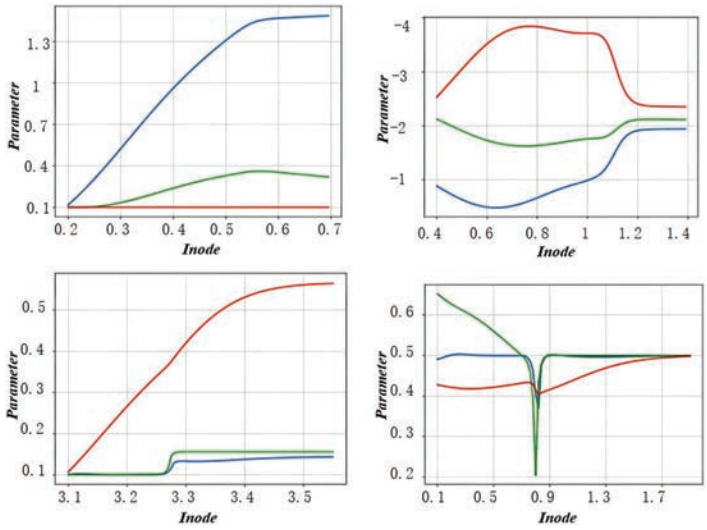

Figure 3 Axdrawing of steel arch of left hole arch.

both sides, the impact of the left hole's lower steps on its axial force surpasses that of the left hole's steel arch frame axial force in the lower section of the right hole. Figure 3 for the left hole arch steel arch shaft diagram, when the right hole steps after the excavation, the first hole in the left wall side steel arch shaft force significantly reduced, when the excavation palm face away from 10 meters, the left hole steel arch shaft force to increase, and the right hole arch steel arch shaft force has been increasing rapidly, the process, the wall side arch waist steel arch force first change, and axial force fluctuations.

When the excavation surface of the right hole extends beyond 40 meters, a gradual decrease is observed in the axial force of the steel arch frame in the left arch and the middle wall of the right hole. Conversely, the axial force of the steel arch frame in other sections continues to ascend until the lower steps reach this point. This phenomenon arises due to the gradual release of stress in the surrounding rock, thereby placing a heavier load on the steel arch. However, as the concrete strength progressively enhances and the initial lining force undergoes constant adjustment, it leads to varied axial force changes across different sections. Upon cutting off the steel arch of the middle guide tunnel, the shaft force of the left hole's steel arch further diminishes, while a slight reduction is observed in the force of the right hole's steel arch. This could be attributed to the relief of the middle wall tilt at this stage. Subsequent to the excavation of the lower steps in the left

hole, a decrease in the pulling axial force of the arch section in both holes is noted, accompanied by an increase in the pressure axial force in other parts. Particularly, the axial force variation is most pronounced at the steel arch's foot in the left hole. as excavation proceeds beneath the steps in the right hole, the axial force in the left hole continues to rise, with minimal change observed in the axial force at the arch foot of the right hole vault and the side wall, while other parts experience an increase. During the excavation process of the lower steps in the main holes on both sides, the influence of the left hole's lower step construction on its shaft force outweighs that of the right hole. Notably, the axial force along the side wall gradually increases from the smallest part to the arch. The maximum axial force in the left hole occurs at the 45° position of the side wall, reaching 147 kN, whereas in the right hole, it occurs at the vault, totaling 169 kN. This discrepancy may be attributed to the excavation process of the main holes on both sides of the arch steps, emphasizing the vulnerability of the arch and side of the middle wall as key tunnel components. Moreover, the significant disparity between the axial force of the side arch and the arch foot suggests potential structural vulnerabilities, particularly if the steel arch at the side arch foot of the middle wall lacks adequate connection with the top of the middle wall, posing a risk of arch collapse. Moreover, the significant disparity between the axial force of the side arch and the arch foot suggests potential structural vulnerabilities, posing a risk of arch collapse. Both left hole and right hole, the wall side arch waist position pulling axial force, and when the main hole on the steps excavation after maximum, the step excavation and two lining, the pulling axial force gradually into pressure axial force, this may be because of the construction, the wall side arch waist position is the weakest part. There is also a pulling axis force in the lower part of the left hole edge wall, but the value is small.

4 Design and Construction of Large-span Continuous-arch Tunnel

4.1 Incremental Constitutive Relation of Large-Span Continuous-Arch Tunnel Design

However, the axial force of the left hole changes greatly in various construction stages, which may be a weak link in the construction, and this part is also vulnerable to disturbance by the construction of the other side hole. In the left hole, when both sides of the main hole steps after excavation, the half of the

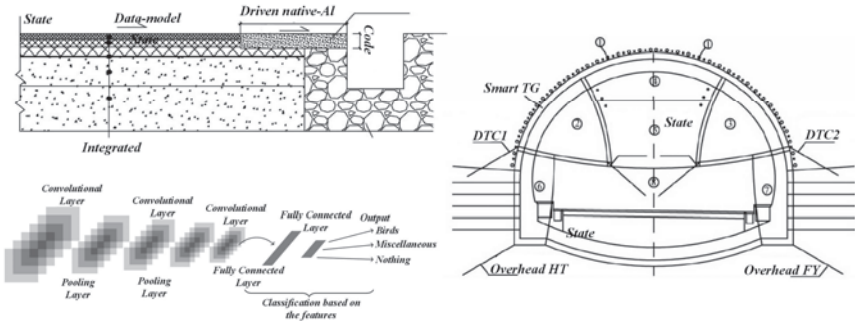

Figure 4 Incremental constitutive relationship diagram of long-span continuous-arch tunnel design.

position of the largest axial force, the steps, the left hole all parts of the axial force are changed, but different parts increase the proportion, the wall side and vault part increase about 1 / 4 of the position, the axial force increase is not big, and the wall side arch waist pulling axial force reduced by half. In the right hole, when the steps of the main holes on both sides are excavated, Figure 4 is the incremental constitutive relationship diagram. The shaft force of the steel arch frame in this part also increases greatly. At this time, the shaft force of each part is larger than that of the corresponding part of the left hole, which may be because the right hole is disturbed before excavation.

During the second lining of the test section, the shaft force of the steel arch frame increased suddenly, and gradually decreased after a few days, and returned to the original value ten days later. After applying the second lining for half a year, the axial force of the steel arch frame has been greatly increased, basically the increase of each part is 1 / 4 of the maximum axial force in the position, and the original pulling axial force also changes into the pressure axial force, indicating that after applying the second lining, the force of the steel arch frame tends to be favorable, that is, the proportion of the axial force difference of each part has decreased. The pulling axial force gradually changes to the pressure axial force, which may be because during the construction, the arch waist of the middle wall is the weakest part. There is also a pulling axis force in the lower part of the left hole edge wall, but the value is small. The axial force of the adjacent parts is greatly different. However, the axial force of the left hole changes greatly in various construction stages, indicating that the force of the steel arch frame of the left hole is more complex than that of the right hole. The axial force of the steel arch frame in the wall of the main hole on both sides changes greatly in each

Table 1 Vault subsidence and peripheral convergence

Arch Class	Excavincrement of Upper Step (cm)	Excavation Increment of the Lower Step (cm)	End Value (cm)
The arch of the left hole sank	3.34	0.23	3.57
The arch of the right hole sinks	3.22	0.20	3.42
The arch of the left hole converges	1.01	0.10	1.11
The lower left hole converges	–	0.03	0.03
The arch of the right hole converges	0.19	0.40	0.59
The lower part of the right hole converges	–	0.16	0.16

construction stage, which may be a weak link in the construction, and this part is also vulnerable to disturbance by the construction of the other side hole. In the left hole, when both sides of the main hole steps after excavation, the half of the position of the largest axial force, the steps, the left hole all parts of the axial force are changed, but different parts increase the proportion, the wall side and vault part increase about 1 / 4 of the position, the steel arch of the axial force increase is not big, and the wall side arch waist pulling axial force reduced by half. In the right hole, when the main holes on the two sides are excavated, the axial force of the steel arch frame in this part increases also greatly. At this time, the axial force of each part is larger than that of the corresponding part of the left hole. This may be because the right hole is excavated after the hole, which is disturbed before excavation.

Because the inverted arch axial force is calculated according to the stress measured by the upper and lower parts of the inverted arch, the axial force will be pulled when the lower part of the inverted arch is pulled. Table 1 shows the subsidence of the vault and the peripheral convergence. After the second lining of the upper part of the left hole, the axial force of the inverted arch of the left hole gradually decreases, indicating that the closed structure is conducive to improving the force of the structure, while the axial force of the right hole increases slightly. When the second lining of the upper part of the right hole, the axial force of the inverted arch of the right hole increases. The increase rate of the axial force is the fastest when the second lining is poured, and then the increase rate decreases slowly, which indicates that the second lining is under force. All axial forces are the final force, the second lining force of the left hole reaches the maximum after half a year, then slightly reduced or remains unchanged, and the other force reaches the maximum after a year.

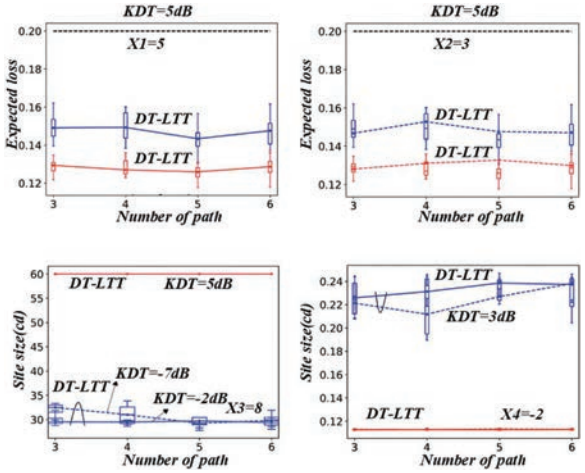

Figure 5 Numerical simulation and evaluation diagram of large-span continuous-arch tunnel.

4.2 Numerical Simulation of a Large-Span Continuous-Arch Tunnel

The arch exhibit some fundamental patterns: in the left hole, the front axial force in the upper arch tends to pull. This tension in the arch shaft might arise due to several factors, including the placement of concrete strain gauges in both upper and lower segments of the inverted arch and the offset of the neutral shaft of the drift arch. Consequently, during stress measurement with instruments, the calculation of the inverted arch shaft force is determined, as depicted in Figure 5 of the numerical simulation evaluation for large-span continuous arch tunnels. In instances where the lower section of the inverted arch experiences tension, the axial force is measured as pulling. The application of the second lining in the upper portion of the left hole, a gradual decrease in the axial force of the left hole is observed. This suggests that the closed structure promotes structural stability.

Following one month, a transition occurs in the axial force of the left hole, gradually shifting towards an axial direction, while concurrently, the axial force of the right hole experiences a gradual increase. Subsequently, after approximately half a year, both holes reach their maximum axial force. Following this peak, there is a slight decline in axial force over the subsequent months, Regarding the basic traits of the axial force concerning the second lining of the inverted arch, there is a gradual increment from zero. Notably, the rate of increase is most rapid immediately after the pouring of the second

Table 2 Comparison of peripheral convergence

		Excavincrement of Upper Step (cm)	Excavation Increment of the Lower Step (cm)	End Value (cm)
The arch of the left	three-dimensional	0.67	2.05	2.72
hole converges	two dimension	1.01	0.10	1.11
The lower left	three-dimensional	–	0.08	0.08
hole converges	two dimension	–	0.03	0.03
The arch of the right	three-dimensional	−0.38	2.43	2.05
hole converges	two dimension	0.19	0.40	0.59
The lower part of the	three-dimensional	–	0.46	0.46
right hole converges	two dimension	–	0.16	0.16

lining. Subsequently, this rate gradually diminishes, indicating a progressive stress build up within the second lining. All axial forces are the final force, the second lining force of the left hole reaches the maximum after half a year, then slightly reduced or remains unchanged, and the other force reaches the maximum after a year. Before the excavation of the main holes on both sides, due to the slight bias, the right vertical pressure is greater than the right side, but the difference is not large; the vertical stress of the middle increases rapidly. Table 2 shows the convergence comparison of the middle wall. In the subsequent construction, and only the stress in the middle wall is linear distribution. It can also be seen from the figure that after the application of the second lining, the height difference between the tunnel exit site and the inlet site is about 60 m, and the minimum main stress in the middle of the middle wall increases by about 6 MPa.

The vertical stress along both sides of the middle wall exhibits uniformity: even when the excavation extends 50 meters away, the vertical stress of the middle wall remains unchanged. However, following the excavation of the tunnel, a slight increase in vertical stress occurs, with the left side registering at 6 MPa. Notably, the most significant axial force variations occur during the main holes on both sides. Conversely, when proceeding the lower steps of these main holes, only a slight increase in axial force is observed.

5 Experimental Analysis

A plane strain model is devised based on authentic data, with a model width set at 120 meters. Vertically, the lower section of the middle guide tunnel

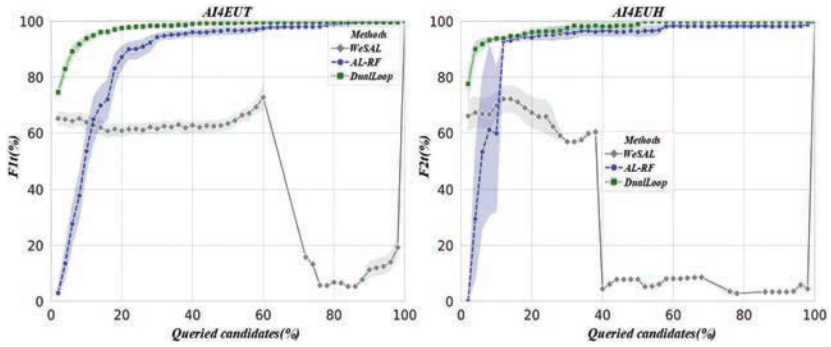

Figure 6 Plar strain model evaluation diagram.

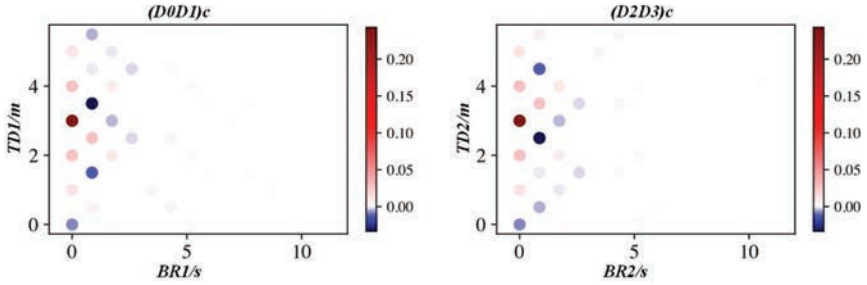

Figure 7 Evaluation drawing of shotcrete.

extends 30 meters beneath the surface, while the upper part of the tunnel conforms to the actual terrain dimensions. The calculation incorporates boundary constraints: Figure 6 illustrates the evaluation diagram of the plane strain model, with the lower boundary constrained by vertical and horizontal displacement.

The contribution of steel mesh and longitudinal connecting bars to the mechanical properties of shotcrete as the safety reserve, which is not considered. The surrounding rock adopts the quadrilateral reference units, the anchor rod adopts the rod unit, and the primary lining and the second lining adopt the beam units. Figure 7 is the evaluation drawing of shotcrete, and the waterproof layer between the primary lining and the second lining adopts the contact surface unit.

The release of ground stress is simulated by applying virtual support force. This model sets: 20% of the wool hole after excavation, 50% after the initial support, and the remaining 30% after the completion of the second lining. Figure 8 shows the evaluation diagram of virtual support force. Since

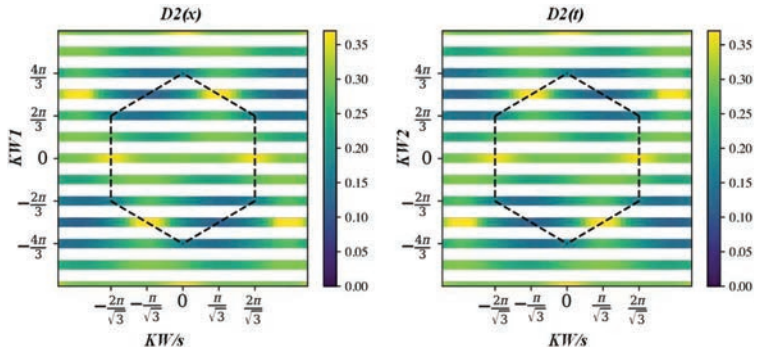

Figure 8 Virtual support assessment diagram.

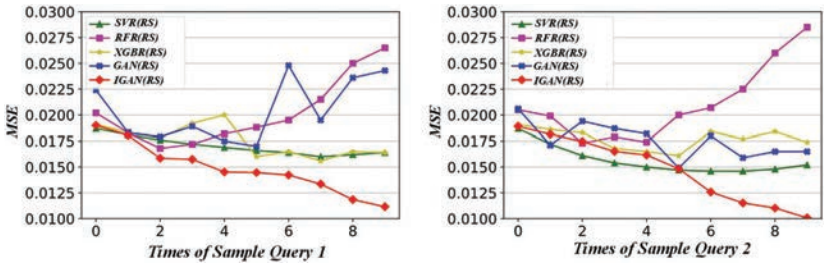

Figure 9 Modeling of tunnel stability control technology.

the tunnel test section is excavated by upper and lower steps, the arch subsidence and surrounding convergence of the main holes on both sides are monitored in the simulation.

Following the excavation of the left tunnel, there is a notable rapid increase in the axial force exerted on the steel arch of the left tunnel's arch. This phenomenon is illustrated in Figure 9, depicting the Modeling of Tunnel Stability Control Technology. Conversely, upon completion of the excavation in the right tunnel's steps, there is a substantial reduction observed in the axial force of the steel arch frame located at the middle wall side of the left tunnel.

As the excavation face approaches within 10 meters, while the axial force in the right tunnel's steel arch frame continues to rise rapidly. Figure 10 illustrates the Numerical Analysis of Tunnel Construction Mechanics, showcasing the dynamics of these forces. During this phase, the waist of the middle wall side arch undergoes initial fluctuations, reaching a distance of 40 meters from the excavation surface in the right tunnel, a discernible trend emerges: the axial force in the steel arch frame of the left tunnel begins to gradually decrease, concomitant with a concurrent increase in the steel in other sections.

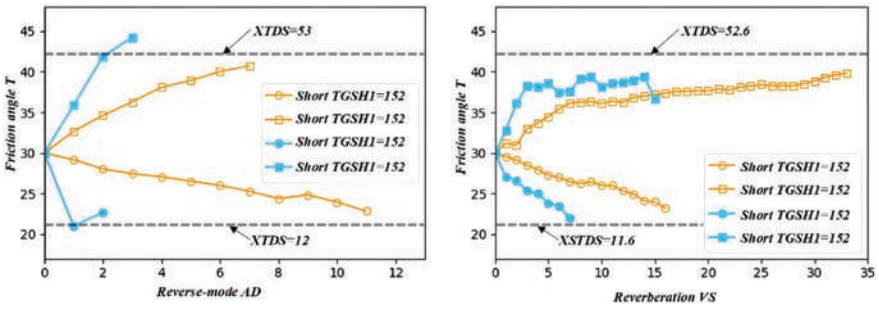

Figure 10 Numerical analysis of tunnel construction mechanics.

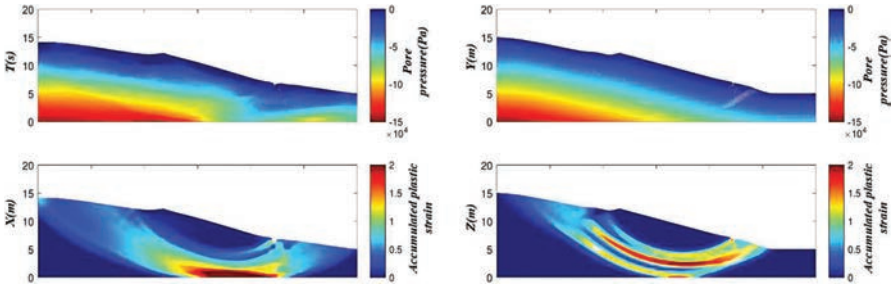

Figure 11 Expressway tunnel stability control.

The steel arch bears a larger load of the surrounding rock, Figure 11 is Expressway Tunnel Stability Control. However, because the concrete strength gradually increases and the initial lining force is constantly adjusted, so it will lead to the increase of axial force in some parts and the decrease of some parts, the right hole arch is slightly reduced, which may be caused by the relief of the middle wall tilt at this time.

6 Conclusion

Subsequently, after the steel arch frame of the middle guide hole is cut off, the tilt of the middle wall towards the first hole side is alleviated. The excavation of the first step results in an increase in the internal force of the initial support for both tunnels. Similarly, following the excavation of the second steps, there is an increase in the internal force of the initial support, albeit with minimal change in the initial support of the arch during this process. Over the initial six months post-second lining application, there is a gradual increase in the internal force of the initial support for both tunnels, followed by a

slight reduction after six months. With the application of the second lining, there is a progressive increase in stress. Initially, the axial force surges rapidly before gradually slowing down, ultimately peaking within a year. The lining of the vault and lower part of the middle wall in both tunnels, along with the side elevation arch of the middle wall, bends towards the headspace, while other parts bend towards the surrounding rock. Notably, in the first tunnel, the axial force of the inverted arch is minor, whereas in the rear tunnel, the axial distribution of the second lining of the cavity differs significantly, Throughout the construction process, the axial force in both main tunnel liners remain compressive. Following the excavation of the steps in both left and right tunnels, there is a notable increase in concrete stress by 55 m, although the concrete stress in both tunnels stabilizes thereafter.

When the steel arch frame of the middle guide tunnel is cut off, the concrete stress, and other parts are not changed. When the left hole lowers the steps, the concrete stress of the left and right holes increases by about 10%; after the excavation of the right hole, the concrete stress of the left hole decreases by about 3%, and the concrete stress of the right hole increases further increased between 9% and 14%. With the approach of the second lining of the left hole (only 10 m), the concrete stress of the two holes begins to decrease; after the second lining of the left hole, the proportion of the increase and the maximum stress is 3%∼12%.

References

[1] Bai, J. R., Lin, Q. H., Bi, H. Y., and Tang, B. M. (2022). Drivers' Eye Movement Characteristics in a Combined Bridge-Tunnel Scenario on a Mountainous Urban Expressway: A Realistic Study. Journal of Advanced Transportation, 2022, 14.

[2] Bao, X., Cui, D. S., Peng, J. L., Liao, M. K., and Zhang, G. C. (2023). Revival Mechanism and Prevention Measures of Composite Landslides: A Case Study of the Wenma Expressway Composite Landslide. Applied Sciences-Basel, 13(4), 19.

[3] Cao, S. D., Xie, Y. L., Tang, W., Wang, W., Zhou, Q. R., and Guo, A. P. (2021). Research on Construction Methods for Ultralarge Y-Shaped Tunnel Sections. Mathematical Problems in Engineering, 2021, 9.

[4] Chen, S. L., and Lee, S. C. (2020). An investigation on tunnel deformation behavior of expressway tunnels. Geomechanics and Engineering, 21(2), 215–226.

[5] Cui, H. J., Chen, G., Zhu, M. Q., Su, Y., and Liu, J. X. (2023). Health State Assessment of Road Tunnel Based on Improved Extension Cloud Model. Applied Sciences-Basel, 13(14), 14.
[6] Hao, Y., Liu, C. H., Zhang, W. C., Liu, X., and Liu, G. H. (2023). Landslide risk evaluation: rainfall and blast-induced potential soil landsides in an expressway area underneath a railway tunnel, Guangzhou, China. Bulletin of Engineering Geology and the Environment, 82(11), 22.
[7] He, Y. R., Chen, P., Ma, W. W., and Chen, C. C. (2020). Construction of 3D Model of Tunnel Based on 3D Laser and Tilt Photography. Sensors and Materials, 32(5), 1743–1755.
[8] Hu, Q. Z., Tang, Y. X., and Ding, Z. G. (2020). Study on the Stability of a Transition Section from Soft to Hard Surrounding Rock Based on the Solid-Fluid Coupling Effect. Advances in Civil Engineering, 2020, 8.
[9] Li, D. D., Xu, H. W., Jiang, T., Ding, H., and Xiang, Y. (2023). Tunnel water burst disaster management engineering based on artificial intelligence technology – taking Yonglian Tunnel in Jiangxi province as the object in China. Water Supply, 23(8), 3377–3391.
[10] Li, J. J., Chen, Q. N., Huang, X. C., Zou, G., and Deng, J. Z. (2021). Pretreatment for Tunnel Karst Cave during Excavation: A Case Study of Guangxi, China. Advances in Civil Engineering, 2021, 12.
[11] Li, J. L., Yuan, C., Zhang, B., and Sui, B. (2021). Evaluation and Application of Surrounding Rock Stability Based on the Improved Weighting Multidimensional Cloud Model. Advances in Civil Engineering, 2021, 9.
[12] Li, Z., Meng, X. Q., Liu, D. W., Tang, Y., and Chen, T. (2022). Disaster Risk Evaluation of Superlong Highways Tunnel Based on the Cloud and AHP Model. Advances in Civil Engineering, 2022, 11.
[13] Li, Z. Q., Lv, S. X., Zhao, J. P., Liu, L. L., and Hu, K. K. (2023). Research on the Experimental System of Reinforcing the Base of Shallow Buried and Wet Collapsible Loess Tunnels. Buildings, 13(7), 20.
[14] Li, Z. Y., Wang, L. Q., Feng, B., Xiao, J., Zhang, Q., Li, L. Y., and Liang, J. (2020). Comprehensive collapse investigation and treatment: An engineering case from qingdao expressway tunnel. Journal of Cleaner Production, 270, 15.
[15] Lin, Z. H., Liu, K. D., Zhang, X. F., Chen, X. G., Xie, P., and Tan, Y. (2023). Optimizations for tunnel drainage water system based on locations of crystallizations. Desalination and Water Treatment, 299, 232–238.

[16] Lin, Z. Q., Gong, W. P., Wan, L., Shen, J. J., Zhang, H., Huang, J., and Zhu, B. B. (2022). Field Measurements for Traffic Noise Reduction in Highway Tunnels Using Closed-Cell Aluminum Foam Board. Applied Sciences-Basel, 12(2), 19.

[17] Liu, K. Y., Guo, J. Q., Wan, L. Y., and Xu, C. (2020). A model test study to optimize the ventilation system of a long expressway tunnel. Journal of Wind Engineering and Industrial Aerodynamics, 207, 16.

[18] Liu, S. Y., Zhang, X. F., Chen, X. G., Wang, C., and Chen, Y. C. (2022). Exploratory Research on Drainage Structure of Highway Tunnel Based on Reducing the Risk of Crystallization Blockage. Processes, 10(7), 14.

[19] Luo, Y. B., Chen, J. X., Shi, Z., Zhang, S. Q., Liu, W. W., and Li, Y. (2020). Mechanical and Deformation Characteristics and Optimization of Support Parameters for Superlarge-Span Tunnel: A Case Study from Laohushan Tunnel. Advances in Civil Engineering, 2020, 17.

[20] Qin, L., Shi, X. H., Leon, A. S., Tong, C. D., and Ding, C. (2020). Dynamic luminance tuning method for tunnel lighting based on data mining of real-time traffic flow. Building and Environment, 176, 10.

[21] Tang, F., Fu, X. S., Cai, M. M., Lu, Y., and Zhong, S. Y. (2021). Investigation of the Factors Influencing the Crash Frequency in Expressway Tunnels: Considering Excess Zero Observations and Unobserved Heterogeneity. Ieee Access, 9, 58549–58565.

[22] Wan, L., Zhou, M., Liu, G., Zhang, C. A., and Yan, Y. (2021). Interactive Influence Analysis of Tunnel Lateral Clearance on Driving Behavior Using Expressway Field Data. Journal of Advanced Transportation, 2021, 15.

[23] Wang, C. Z., Easa, S., Chen, F., and Cheng, J. C. (2023). Spatiotemporal Evaluation of Injury Severity of Expressway Rear-End Crashes in China: Insights Using Random Parameters Approaches. Transportation Research Record, 21.

[24] Wang, F., Gu, D. J., Li, Y. Y., Liu, W., Wang, G. Y., and Ding, N. K. (2021). Effects of Visual Active Deceleration Devices on Controlling Vehicle Speeds in a Long Downhill Tunnel of an Expressway. Applied Sciences-Basel, 11(15), 18.

[25] Wang, J. X., Cao, A. S., Wu, Z., Sun, Z. P., Lin, X., Sun, L., … Sun, Y. W. (2022). Numerical Simulation of Ultra-Shallow Buried Large-Span Double-Arch Tunnel Excavated under an Expressway. Applied Sciences-Basel, 12(1), 24.

[26] Wang, L., Chen, X. X., and Chen, H. (2020). Influencing Factors on Vehicles Lateral Stability on Tunnel Section in Mountainous Expressway under Strong Wind: A Case of Xi-Han Highway. Advances in Civil Engineering, 2020, 11.

[27] Wang, L., Li, S. Q., and Hui, B. (2021). Simulation Analysis of the Distance Between Tunnels at the Bridge-Tunnel Junction of Mountainous Expressway on Driving Safety Under Crosswinds. Ieee Access, 9, 28514–28524.

[28] Wu, F. Y., He, C., Yang, W. B., Kou, H., Chen, Z. Q., Wang, F., and Meng, W. (2022). Engineering behavior of soft rock tunnels in mountainous areas under multiple hazard inducers: a case study of the Jiuzhaigou-Mianyang Expressway. Bulletin of Engineering Geology and the Environment, 81(8), 27.

Biographies

Wei Li received the Bachelor's degree in Engineering from Taiyuan University of Technology in 2004, the Master's degree in Engineering form Taiyuan University of Technology in 2012. He is currently working as an associate professor in the College of Engineering Management, Shanxi Vocational University of Engineering Science and Technology. His research areas and directions include mechanics, Road and bridge engineering.

Hongping Wen received the Bachelor's degree in Engineering from Chang'an University of Technology in 2010, the Master's degree in Engineering form Chang'an University in 2013. He is currently working as an associate professor in the College of Engineering Management, Shanxi Vocational University of Engineering Science and Technology. His research areas and directions include mechanics, materials, and structures.